Electrophysiological and Pharmacological Characterization of Human Inwardly Rectifying $K_{ir}2.1$ Channels on an Automated Patch-Clamp Platform

Camille Sanson,[1] Brigitte Schombert,[1] Bruno Filoche-Rommé,[2] Michel Partiseti,[1] and G. Andrees Bohme[1]

[1]Integrated Drug Discovery, High-Content Biology, Sanofi Research and Development, Vitry-sur-Seine, France.
[2]Integrated Drug Discovery, Medicinal Chemistry, Sanofi Research and Development, Vitry-sur-Seine, France.

ABSTRACT

Inwardly rectifying I_{K1} potassium currents of the heart control the resting membrane potential of ventricular cardiomyocytes during diastole and contribute to their repolarization after each action potential. Mutations in the gene encoding $K_{ir}2.1$ channels, which primarily conduct ventricular I_{K1}, are associated with inheritable forms of arrhythmias and sudden cardiac death. Therefore, potential iatrogenic inhibition of $K_{ir}2.1$-mediated I_{K1} currents is a cardiosafety concern during new drug discovery and development. $K_{ir}2.1$ channels are part of the panel of cardiac ion channels currently considered for refined early compound risk assessment within the Comprehensive in vitro *Proarrhythmia Assay initiative. In this study, we have validated a cell-based assay allowing functional quantification of $K_{ir}2.1$ inhibitors using whole-cell recordings of Chinese hamster ovary cells stably expressing human $K_{ir}2.1$ channels. We reproduced key electrophysiological and pharmacological features known for native I_{K1}, including current enhancement by external potassium and voltage- and concentration-dependent blockade by external barium. Furthermore, the K_{ir} inhibitors ML133, PA-6, and chloroquine, as well as the multichannel inhibitors chloroethylclonidine, chlorpromazine, SKF-96365, and the class III antiarrhythmic agent terikalant demonstrated slowly developing inhibitory activity in the low micromolar range. The robustness of this assay authorizes medium throughput screening for cardiosafety purposes and could help to enrich the currently limited $K_{ir}2.1$ pharmacology.*

Keywords: safety pharmacology, CiPA initiative, sudden death, torsades de pointes, K^+ channels, ventricular arrhythmia

INTRODUCTION

Inhibition of the voltage-dependent potassium channels $K_v11.1$, also referred to as human Ether-à-go-go Related Gene (hERG), which mediates the delayed rectifier I_{Kr} potassium current in the heart, has been identified in the 1990's as a central mechanism associated with "Torsades de Pointe" (TdP) arrhythmias and sudden cardiac death. This major cardiosafety issue caused the market withdrawal of a significant number of pharmaceuticals.[1] Disruption of hERG function slows the repolarization phase of the cardiac action potential (AP), increasing its duration and favoring the initiation of early after depolarizations and ventricular arrhythmia, which can degenerate in TdP.[2] In accordance with internationally harmonized guidelines,[3,4] these findings prompted the systematic early cardiosafety benefit/risk assessment of new drug candidates through evaluation of their functional effects at hERG channels *in vitro*, along with action potential duration (APD) measurements in *ex vivo* ventricular conductive tissue preparations such as rabbit Purkinje fibers.[5,6] These studies are combined with *in vivo* measurements of the time interval between Q-wave and T-wave (QT) on the electrocardiogram, typically conducted in conscious dogs,[6,7] and are followed as appropriate by specific thorough QT (TQT) studies during the early clinical development phases.

Despite the fact that these guidelines resulted in no further drugs being withdrawn from the market for arrhythmia liabilities since their implementation, the consistency of the surrogate markers examined as unequivocal predictors of TdP risk has recently been challenged. In addition, their stringency when taken individually as compound prioritization criteria may have generated unnecessary attrition of otherwise efficient and innovative drugs. For example, it has been shown that among nearly one hundred preclinical compounds, hERG inhibition translates into APD prolongation in only half of the cases, with one-third revealing no activity on APD, and one-sixth actually shortening it. Moreover, it was shown that drugs either prolonging or shortening the APD could produce ventricular arrhythmia, at least in excised hearts.[8] Similarly, a retrospective analysis of several tens of advanced candidates, which underwent TQT studies in humans, showed that the predictive value of hERG inhibition alone, while being sensitive, substantially lacks specificity.[9]

Hence, several drugs from various pharmacological classes with diverse chemical structures do not induce proarrhythmia in clinical practice, despite being significant hERG inhibitors at therapeutically relevant concentrations. Kramer *et al.*[10] suggested that, for many of these drugs, the discordance could result from compensatory inhibitory activities at depolarizing cardiac ion channels other than hERG contributing to shape the AP. Specifically, it was shown that among 55 small molecules with a clinically documented high or low TdP risk, additional inhibitory activity at $Ca_V1.2$-mediated $I_{Ca,L}$ calcium currents (and to a lesser extend at $Na_V1.5$-mediated I_{Na} peak sodium currents) better describes their cardiosafety profile compared to knowledge of hERG inhibition alone.

The ongoing comprehensive *in vitro* proarrhythmia assay (CiPA) initiative is a public–private collaboration put in place a few years ago with the objective to propose better ways to predict the proarrhythmic potential of preclinical compounds. This endeavor proposes to address the cardiosafety risk of a compound by combining its inhibitory profile at multiple cardiac ion channels with the predictions of an *in silico* model of human ventricular electrophysiology previously trained with the inhibitory profile of clinical drugs with documented high, medium, or low torsadogenic potential. The predictions would then be optionally compared with actual measurements on stem cell-derived cardiomyocytes before being assessed by electrocardiography monitoring during the early phases of clinical development. The panel of channels selected for the CiPA profiling comprise the depolarizing $Ca_V1.2$- and $Na_V1.5$-mediated $I_{Ca,L}$ and I_{Na} peak and late currents, as well as the repolarizing $K_v11.1$-, $K_v7.1$-, $K_v4.3$-, and $K_{ir}2.1$-mediated I_{Kr}, I_{Ks}, I_{to}, and I_{K1} currents.[11–15] In this study, we have developed a medium throughput screening assay based on automated whole-cell patch-clamp recording of $K_{ir}2.1$-mediated I_{K1} currents.

Inwardly rectifying $K_{ir}2.1$ potassium channels belong to a family of transmembrane proteins sharing the property to flux K^+ ions more readily in the inward than in the outward direction. This "biological diode"-like behavior is linked to their voltage-dependent block by cytoplasmic polyamines or magnesium ions, which plug their conduction pore at depolarized voltages.[16,17] $K_{ir}2.1$ and other members of the $K_{ir}2.x$ subfamily display strong rectification properties and contribute thereby to the control of the membrane resting potential in excitable tissues by constantly dragging the membrane toward the K^+ equilibrium potential E_K. They also support repolarization following AP firing (reviewed in refs.[18–21]).

Despite the dearth of selective and potent pharmacologic agents,[22] and the fact that several different $K_{ir}2.x$ subunits expressed in the heart can assemble into functional heterotetramers,[23] convergent lines of evidence concur to support a primary role for $K_{ir}2.1$ subunits to conduct I_{K1} in cardiac ventricles. First, I_{K1} currents are significantly reduced in rat ventricular cardiomyocyte exposed to antisense oligonucleotides targeting $K_{ir}2.1$ mRNAs.[24] Second, no I_{K1} currents can be recorded from cardiac cells in neonate $K_{ir}2.1$ knockout mice during the few hours they survive.[25] Third, I_{K1} can be enhanced or decreased in guinea pig hearts treated with adenovirus encoding wild-type $K_{ir}2.1$ or a dominant-negative mutant $K_{ir}2.1$ protein, respectively.[26] Fourth, a clear translational path links rare human hereditary diseases involving loss- or gain-of-function mutations in the *KCNJ2* gene encoding $K_{ir}2.1$ subunits with cardiac rhythm abnormalities.[27,28]

One important aspect of the evaluation of drug effect at multiple cardiac ion channels pertains to adopting profiling methods reliably assessing the intrinsic activity of test articles using unbiased functional readouts. Authier *et al.*[29] recently published a survey on current practices in the pharmaceutical industry, indicating that patch-clamp electrophysiology on human ion channels expressed in cell lines is the most common approach to the CiPA ion channel strategy. The development in the last decade of automated planar patch-clamp systems providing gigaseal quality recordings allows sufficient throughput to adequately expedite early cardiosafety support for the curtailed optimization cycles of modern medicinal chemistry. In this study, we undertook the validation of a $K_{ir}2.1$ assay on such a platform, allowing rapid quantification of drug inhibitory activity to complement an integrated drug discovery cardiosafety liability assessment panel.

MATERIALS AND METHODS

$K_{ir}2.1$ Cell Line

A Chinese hamster ovary (CHO) cell line stably expressing the human *KCNJ2* gene product (GenBank NM_000891.2) under the control of a tetracycline-inducible promoter was obtained from a commercial source and cultivated according to the vendor instructions (Charles River; Cat. No. CT6127). The cells were grown in a humidified 95% air/5% CO_2 atmosphere in Dulbecco's modified Eagle's medium/F-12 Nutrient Mixture (ThermoFisher Scientific) supplemented with 10% fetal bovine serum and the appropriate selection antibiotics (0.01 mg/mL blasticidin and 0.4 mg/mL zeocin). For stock cultures, cells were grown in T175 flasks and passaged every 3–4 days below 80% confluence. Cell detachment was obtained by exposure to TrypLE Select™ (Gibco, ThermoFisher Scientific) for 2–3 min at 37°C. Flasks prepared in view of electrophysiological recordings were typically seeded 2 days before the experiments with an inoculum containing about 2.5 million cells per T175 flask filled with 25–30 mL growth medium. Expression of the $K_{ir}2.1$ channels was obtained by overnight induction with 1 μg/mL doxycycline added to the growth medium. On the day of recording, detached cells were spun down, washed, resuspended to 5–8 million cells/mL in a glucose-containing extracellular buffer, and placed in the cabinet of a QPatch® 48X workstation (Sophion Bioscience, Denmark). This standalone instrument comprises a robotic pipetting arm ensuring distribution of cell suspensions into disposable 48-well recording plates (QPlates®) and the sequential application of drug solutions at final test concentration, while whole-cell patch-clamp is maintained without interruption.[30]

Automated Patch-Clamp

All recordings were performed at room temperature. Experiments aimed at characterizing the electrophysiological properties of the currents were conducted on biochips endowed with a unique pinhole orifice engineered at the bottom of each of the 48 wells of disposable measurement plates (i.e., single-hole QPlates). Currents were activated by application of a series of 500 ms-long square voltage pulses delivered every 90 s and incremented in 5 mV steps from a holding potential of −20 mV. Currents measured over 30 ms at the end of each step served to plot current-voltage (I–V) relationships. In some experiments, the external potassium $[K^+]_{out}$ concentration was changed, while maintaining internal $[K^+]_{in}$ constant to change the K^+ equilibrium potential. In other single-hole recordings, the I–V relationships were established in an external buffer supplemented with various concentrations of alkaline or alkaline-earth metal ions.

Experiments aimed at characterizing the pharmacology of small molecules were conducted with 48-well measurement plates, each fitted with biochips perforated with 10 holes, so that each recording site sums up the signal from multiple cells (i.e., multi-hole QPlates). The voltage protocol used was a step-ramp protocol applied every 30 s, which first stepped the membrane from a holding potential of −20 mV down to −120 mV for 500 ms, then ramped it up to 0 mV over 1 s, and eventually stepped the membrane potential back to −20 mV, where the cells were held until the next voltage cycle. This protocol allowed for long-time (30 min) recordings comprising a stable baseline and ample space for the application of multiple drug concentrations in a row. Moreover, the voltage ramp permitted to check the recording quality over time by monitoring the stability of the zero-current reversal potential value. The size of the inward current measured at the end of the initial hyperpolarizing 500 ms-step to −120 mV was used to evaluate drug effect.

For all experiments, the intracellular recording buffer contained (in mM) 5.37 $CaCl_2$, 1.75 $MgCl_2$, 10 ethylene glycol tetraacetic acid, 10 HEPES, 120 KCl, and 4 Na_2-ATP (pH 7.2, 300 mOsm) and the standard extracellular recording buffer contained (in mM) 2 $CaCl_2$, 1 $MgCl_2$, 10 HEPES, 4 KCl, 145 NaCl, and 10 Glucose (pH 7.4, 310 mOsm).

Drugs

All test articles were from Sanofi's internal libraries, except ML133 (CAS Number 1222781-70-5; Wang *et al.*[31]), which was obtained from a commercial source (Sigma-Aldrich, Saint-Quentin-Fallavier), and PA-6 (CAS Number 1199627-07-0, Takanari *et al.*[32]), a pentamidine derivative, which was synthesized following published procedures and references therein.[32,33] *Figure 5* depicts the structural formula and IUPAC chemical names of ML133, PA-6, and the five other small-molecule inhibitors examined in this study. Compounds were dissolved as 10, 50, or 100 mM concentrated stocks in dimethyl sulfoxide (DMSO) using sonication as needed for complete dissolution, then aliquoted into capped polypropylene vials, and kept frozen at −20°C until use. On the day of study, stock solutions were diluted to the final concentrations intended for cell applications in standard 96-well microtiter plates (MTP) containing the extracellular buffer supplemented with 0.06% Pluronic F-68™ (Gibco, ThermoFisher Scientific). The latter surfactant was added to help slow unseen precipitation (if any) of poorly soluble drugs in the MTP wells upon dilution.[34] The final drug solutions also contained 0.3% residual DMSO from the dilution processes. The test article solutions were typically applied to the cells within 30 min of preparation. Concentration–response data were either

obtained from the cumulative applications of six increasing concentrations to the same cells within a given recording well, each concentration being exposed for 3 min, or by applying a single different concentration into given wells with an exposure duration extended to 15 min.

Data Handling

Current amplitude measurements and normalization for the fitting of concentration–response curves were done with Sophion's dedicated analysis software (Odense 5.6.4). Time course of current amplitude was visualized offline and analyzed following optional rundown compensation as needed using built-in routines proprietary to this software (uncorrected rundown measured in $N = 5$ vehicle-treated cells did not exceed 1% per min in single application experiments). All recordings for pharmacological determinations were concluded by the application of a supramaximal concentration (3 mM) of barium as full block. Residual leak currents remaining under full block (if any) were subtracted from precedent data points. A professional graphing package (Prism 7.02; GraphPad Software) was used for drawing exported current traces, plotting I–V curves, and performing statistical calculations. Half-maximal inhibitory concentrations (IC_{50}) were obtained by fitting the average of the two or the five last current amplitude readings at the end of each drug concentration exposure period in a cumulative or noncumulative application mode, respectively. A classical four-parameter Hill equation following normalization with respect to predrug baseline readings was used for data fitting to a sigmoidal curve with minimum and maximum constrained to 0% and 100%, respectively. Estimated IC_{50} and Hill coefficient (n_H) values are reported along with their estimated 95% confidence interval (CI). Mean of individual replicates is represented with their calculated standard deviations shown as error bars on graphs where appropriate.

RESULTS AND DISCUSSION

Electrophysiological Characterization

The upper part of *Figure 1A* illustrates the typical appearance of whole-cell currents recorded from stably transfected CHO cells induced to express the human *KCNJ2* gene product. Inward or outward currents reaching steady state within a 100 ms developed when the membrane was stepped tens of mV below or above the K^+-equilibrium potential (E_K), respectively (*Fig. 1A*). At more depolarized potentials, the current–voltage (I–V) relationship displayed a strongly inward rectifying profile. This profile fully concurs with the I–V outline of native ventricular I_{K1} currents.[35] Specifically, the amplitudes of the inward currents below E_K grew linearly in proportion to the negativity of the membrane, reaching relatively large values at strong hyperpolarization (*e.g.*, -2.3 ± 0.4 nA at -120 mV, $N = 10$, *Fig. 1B*), whereas the positive currents above E_K culminated at potentials around -60 to -50 mV (*e.g.*, 0.31 ± 0.09 nA at -60 mV, $N = 10$, *Fig. 1B*). Virtually no currents were detected in induced cells at potentials more positive than -20 mV (*Fig. 1B*) nor at any potential in noninduced CHO cells (*Fig. 1A* bottom), even when the latter were stepped to very negative potentials (*e.g.*, 0.07 ± 0.05 nA at -120 mV, $N = 10$), indicating the absence of endogenous I_{K1}-like currents in the host CHO cell line. The success rate of exploitable recordings obtained from single-hole QPlates routinely exceeded half of the 48

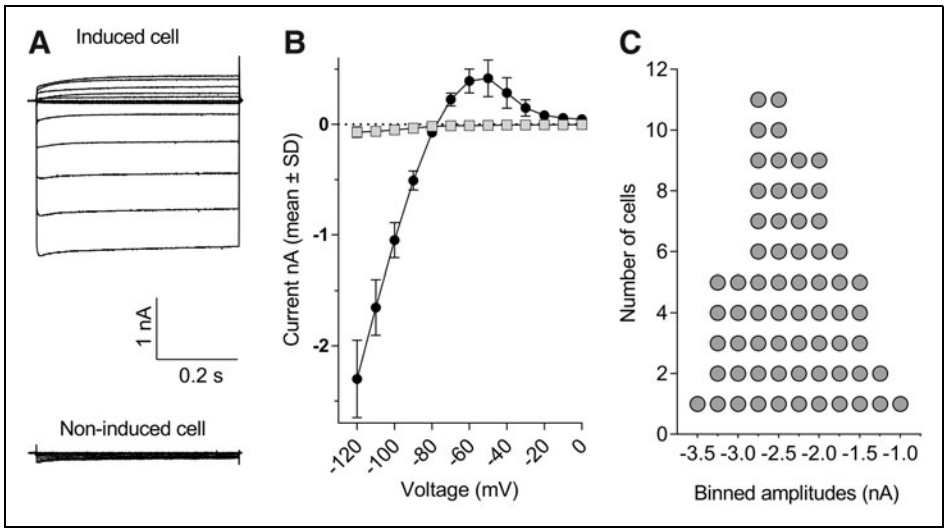

Fig. 1. Inward and outward currents in CHO cells stably expressing the human *KCNJ2* gene recorded with single-hole QPlates. **(A)** Family of representative current traces obtained by stepping the membrane from a holding of −20 mV to voltages ranging from −120 to 0 mV in a cell exposed overnight to doxycycline (*top left*) or in a noninduced cell (*bottom left*). **(B)** Mean steady-state currents plotted as a function of voltage for $N = 10$ induced (*closed circles*) and noninduced (*gray squares*) cells. Error bars represent standard deviation and are smaller than symbol size in noninduced cells. **(C)** Descriptive statistics of steady-state current size at −120 mV collected from $N = 65$ cells sampled from three single-hole QPlates. Frequency distribution was constructed at a binwidth of 0.25 nA. CHO, Chinese hamster ovary.

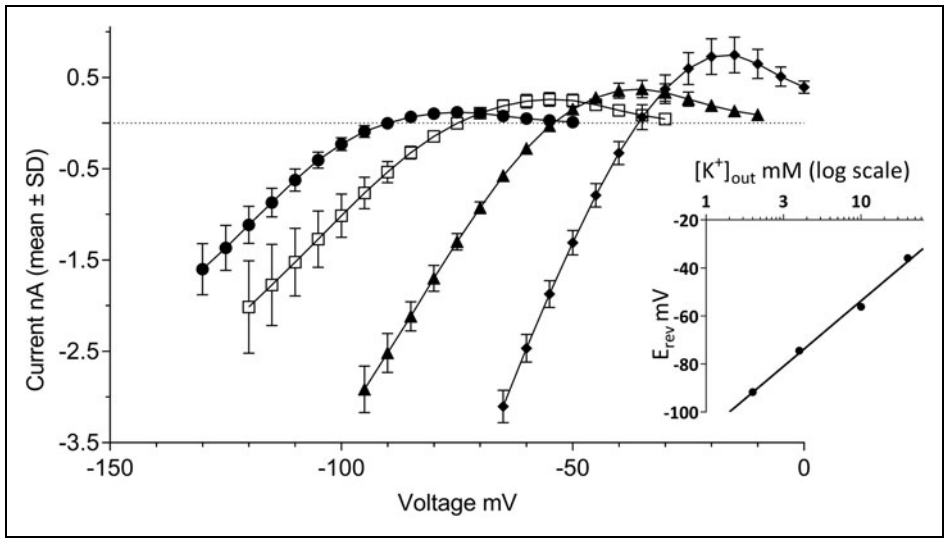

Fig. 2. Potassium selectivity of the currents in *KCNJ2* expressing CHO cells. The graph shows I–V relationships established in external recording buffer containing various $[K^+]_{out}$ concentrations. Steady-state currents were recorded in $[K^+]_{out} = 2$ mM (*closed circles*), $[K^+]_{out} = 4$ mM (*open squares*), $[K^+]_{out} = 10$ mM (*closed triangles*), or $[K^+]_{out} = 20$ mM (*closed diamonds*). Error bars represent standard deviation for data derived from $N = 5$–10 cells. The *inset* depicts a linear regression fit of the $\log_{10}$ of $[K^+]_{out}$ concentration to the membrane potential values at which no current is observed (i.e., zero-current reversal potential).

wells. For example, statistics derived from $N = 3$ single-hole QPlates indicated that, from 126 cells, which successfully entered whole-cell mode (*i.e.*, 88% of the 144 theoretically possible), a total of $N = 65$ cells formerly exhibiting seal resistances well above 200 MΩ provided complete I–V curves after 30-min recording, demonstrating that 52% of the cells recovered satisfactorily from clamp engagement and remained stable during repeated voltage stepping cycles. *Figure 1C* illustrates the current size frequency distribution for this sample of 65 cells. The median inward steady-state current amplitude at −120 mV was −2.4 nA, along with an interquartile range spreading from −1.7 to −2.9 nA.

A prominent property of currents flowing through $K_{ir}2.x$ channels is their activation by external potassium $[K^+]_{out}$. This counterintuitive behavior (given the decreased electrochemical gradient when $[K^+]_{out}$ is increased) results from an increased open-channel conductance in response to elevation of external K^+.[36] In the experiments illustrated in *Figure 2*, $[K^+]_{out}$ was varied over four concentrations ranging from 2 to 20 mM, while internal potassium was kept constant at $[K^+]_{in} = 120$ mM. The I–V relationships outlined by the four pairs of buffers exhibited a rightward shift proportional to $[K^+]_{out}$, along with a concomitant increase in the size of both the inward and outward currents. The latter culminated at 0.12 ± 0.06, 0.26 ± 0.08, 0.37 ± 0.10, and 0.74 ± 0.20 nA when the external buffer contained 2, 4, 10, and 20 mM $[K^+]_{out}$, respectively ($N = 5$–10 cells per condition, *Fig. 2*). Beyond these maxima, the I–V curves presented regions of negative slope conductance until complete extinction of the currents. Their steepness was also proportional to $[K^+]_{out}$, and the superposition of the outward currents in these voltage regions of the I–V curves draw a series of typical "cross-over" patterns as previously described by others.[35,37] In response to the increasing $[K^+]_{out}$, the zero-current potential of each I–V relationship shifted rightward from -92 ± 1.2 mV at 2 mM $[K^+]_{out}$ to -75 ± 2.7 mV, -56 ± 1.5 mV, and -36 ± 1.2 mV for 4, 10, and 20 mM $[K^+]_{out}$, respectively. Linear regression of these data as a function of log $[K^+]_{out}$ yielded a highly significant ($r^2 = 0.992$) fit (*Fig. 2*, inset) with an estimated 54 ± 3.4 mV shift of the zero-current potential per tenfold variation of external $[K^+]_{out}$, in good agreement with the Nernst equation prediction of 58 mV per decade.

Taken together, the electrophysiological features summarized in *Figures 1* and *2* demonstrate rectification properties and activation by external potassium typical of $K_{ir}2.1$-mediated I_{K1} currents. Of note, the high yield of decent currents collected simultaneously allowed to expedite the characterization of a number of electrophysiological features with minimal need of experiments.

Pharmacological Characterization

Cations such as Cs^+ and Ba^{2+} are blockers of native I_{K1} currents in sheep Purkinje fibers,[38] starfish eggs,[39,40] or frog leg muscles,[41] abolishing the influence of $[K^+]_{out}$ on the I–V profile and blocking I_{K1} in a concentration- and voltage-dependent manner. These cations are fast-acting open-channel blockers, reaching steady-state inhibition of the current flow within a few seconds after external exposure. This property was used to document $K_{ir}2.1$ channels when they were first isolated by expression cloning in *Xenopus* oocytes. *Figure 3* illustrates the effects of micromolar Ba^{2+} concentrations on $K_{ir}2.1$-mediated I_{K1} currents activated by a

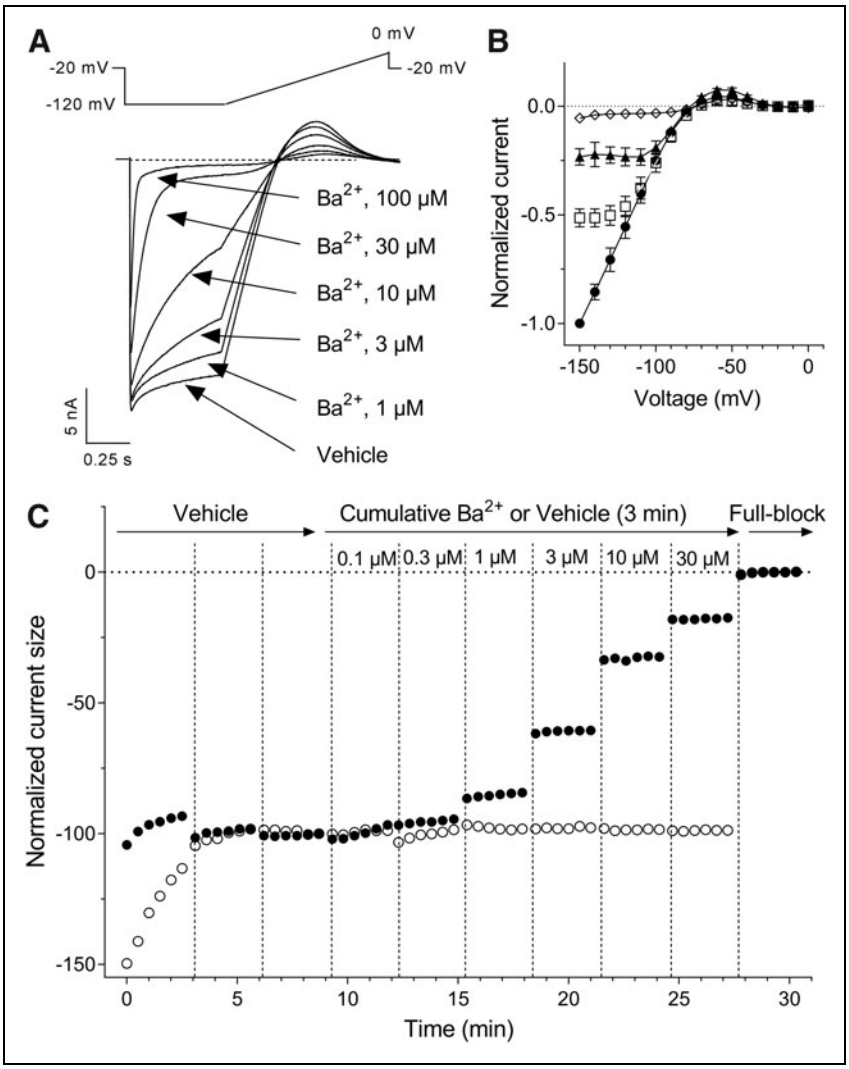

Fig. 3. Sensitivity of K^+ currents in *KCNJ2* expressing cells to external Ba^{2+} ions. **(A)** Representative current traces recorded in a multi-hole QPlate, which groups signal derived from up to 10 cells in response to the voltage protocol schematized above the traces. **(B)** Normalized I–V relationships derived from $N=3$ cells recorded in a single-hole plate in the absence (*closed circles*) or presence of 3 μM Ba^{2+} (*open squares*), 10 μM Ba^{2+} (*closed triangles*), or 100 μM Ba^{2+} (*open diamonds*) showing concentration and voltage dependency of $K_{ir}2.1$ blockade by external Ba^{2+}. Error bars represent standard deviations. **(C)** Plot of steady-state current amplitude normalized with respect to baseline. Cells were exposed to successive vehicle control or test-article liquid application episodes, each of 3-min duration as indicated by *vertical dashed line*. Currents were activated by repeated application of the same step-ramp protocol as in **(A)**. Control experiment (*open circles*) consisted in nine repeated applications of vehicle alone. Treatment experiment (*closed circles*) consisted in applications of vehicle buffer containing $BaCl_2$ at the indicated concentrations. The average two measurements at the end of the last vehicle period and at the end of each drug period served for current amplitude normalizations. Recordings were terminated by application of a saturating concentration of Ba^{2+} (3 mM) as full block.

step-ramp voltage protocol in *KCNJ2* expressing CHO cells. As previously described by Kubo *et al.*,[42] external Ba^{2+} blocked the steady-state current more strongly toward the end of the hyperpolarizing pulses than the initial instantaneous current (*Fig. 3A*). Moreover, this time-dependent inhibition was also voltage dependent, the channel block increasing when the membrane was stepped to more negative potentials (*Fig. 3B*). Group data obtained from $N=3$ single-hole recordings indicated that the inhibition of the inward current produced by 3 μM Ba^{2+} reached 17% at −120 mV, increasing to 48% at −150 mV. Similarly, the 58% inhibition of the current afforded by 10 μM Ba^{2+} at −120 mV rose to 77% at −150 mV. These properties result in characteristic changes in the I–V relationship profile in the presence of Ba^{2+} (*Fig. 3B*) and Cs^+ ions (data not shown). *Figure 3C* depicts the time course of the effect of cumulative applications of increasing concentrations of Ba^{2+} into a multi-hole recording well. The $K_{ir}2.1$-mediated I_{K1} currents stabilized within several minutes after whole-cell access. As expected from a fast-acting pore blocker, the inhibitory effect of each cumulatively applied concentration of Ba^{2+} fully developed within the first couple of voltage-protocol cycles immediately at the beginning of each 3-min application period. The IC_{50} value (calculated from the average normalized inward current amplitudes collected at the two last voltage steps down to −120 mV of each incubation period) was estimated at 8.2 μM (95% CI: 7.6–8.8 μM, $N=6$, *Fig. 4*). The Hill coefficient (n_H) associated to the sigmoidal fit of the normalized data was close to unity ($n_H=1.03$; 95% CI: 0.96–1.1), consistent with a mechanism involving a single ion blocking each channel pore according to first-order kinetics. Notwithstanding the voltage dependency of the blocking effect of Ba^{2+}, this value is in fairly good agreement with published values on $K_{ir}2.1$ currents recorded in HEK cells (IC_{50} = 7.9 μM at −90 mV, Shen *et al.*[43]) or *Xenopus* oocytes (IC_{50} = 16 μM at −120 mV, Schram *et al.*[23]). The time course and the inhibitory effects of Cs^+ and Sr^{2+} ions using the same cumulative concentration–response application protocol were very similarly to Ba^{2+},

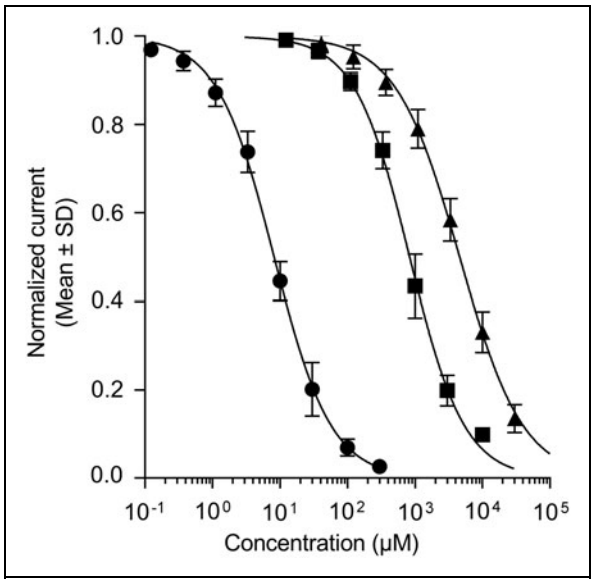

Fig. 4. Inhibition of $K_{ir}2.1$-mediated I_{K1} currents by alkali or alkaline-earth channel blockers. Ba^{2+} (*circles*), Cs^{+} (*squares*), and Sr^{2+} (*triangles*) ions were tested as chloride salts in multi-hole QPlates. Group estimates were derived from at least $N=3$ wells from overlapping concentration ranges applied cumulatively to the same cells (see legend to *Fig. 3C* and text for details and estimated IC_{50} values with 95% confidence intervals). IC_{50}, half-maximal inhibitory concentrations

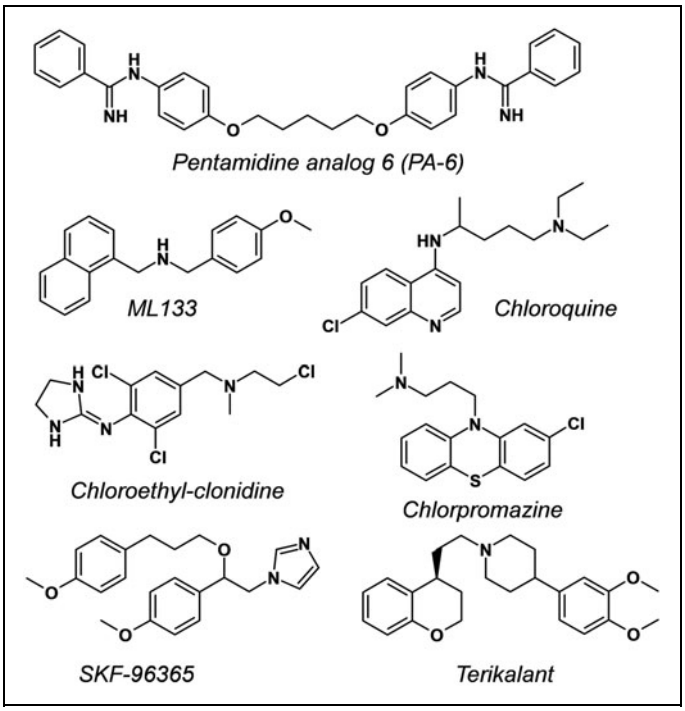

Fig. 5. Chemical structure of disclosed compounds with $K_{ir}2.1$ inhibitory properties evaluated in this study: PA-6, *N*,*N*′′-((pentane-1,5-diylbis(oxy))bis(4,1-phenylene)) dibenzimidamide[32]; ML133, *N*-(4-methoxybenzyl)-1-(naphthalene-1-yl) methanamine[31]; Chloroquine, 4-*N*-(7-chloroquinolin-4-yl)-1-*N*,1-*N*-diethylpentane-1,4-diamine[46]; Chloroethylclonidine, *N*-[2,6-dichloro-4-[[2-chloroethyl(methyl)amino] methyl]phenyl]-4,5-dihydro-1H-imidazol-2-amine[50]; Chlorpromazine, 3-(2-chlorophenothiazin-10-yl)-*N*,*N*-dimethylpropan-1-amine[51]; SKF-96365, 1-[2-(4-methoxyphenyl)-2-[3-(4-methoxyphenyl)propoxy]ethyl] imidazole[52]; Terikalant, 1-[2-[(4S)-3,4-dihydro-2H-chromen-4-yl]ethyl]-4-(3,4-dimethoxyphenyl)piperidine.[53]

exhibiting full inhibitory activity immediately at the beginning of each application period. These blockers were less potent than Ba^{2+}, yielding IC_{50} values of 833 μM (95% CI: 789–880 μM, $N=12$) with $n_H=1.07$ (95% CI: 1.0–1.1), and 4,585 μM (95% CI: 4,308–4,881 μM, $N=11$) with $n_H=0.92$ (95% CI: 0.87–0.98), respectively (*Fig. 4*). The potency obtained for Cs^{+} on human $K_{ir}2.1$ channels was one order of magnitude weaker than published data for mouse $K_{ir}2.1$ overexpressed in a murine erythroleukemia cell line ($IC_{50}=91$ μM at −100 mV, Abrams *et al.*[44]), raising the possibility that $K_{ir}2.1$ expression in a conspecific rather than ectopic cell environment affects voltage dependency of Cs^{+} blockade. We did not find quantitative pharmacological data with which to compare our potency determinations for Sr^{2+} ions.

There are currently no selective small-molecule $K_{ir}2.1$ inhibitors with nanomolar potency described in the literature.[22] Even in the realm of toxins isolated from the venom of poisonous species, which are a rich source of high affinity ion channel modulators, no $K_{ir}2.1$ selective peptide inhibitors have been described so far.[45] We therefore went on to characterize the pharmacology of the $K_{ir}2.1$-mediated I_{K1} currents expressed in CHO cells using seven small-molecule inhibitors displaying micromolar potencies in manual patch-clamp experiments (*Fig. 5*). We started with the aromatic diamidine derivative PA-6,[32] the methoxybenzyl-methanamide ML133,[31] and the antimalaria drug chloroquine[46] using the six-point cumulative application paradigm adopted with Ba^{2+} and the other ionic pore blockers. However, the active concentrations of these weak amines did not reach full inhibition within the 3-min exposure periods. Previous studies comparing the inhibitory activity of these compounds in the inside-out and whole-cell patch-clamp configurations evidenced an accelerated inhibition rate and increased potency against $K_{ir}2.1$ currents when excised patches were assayed. These data pointed to cytoplasmic sites of actions for these three compounds, and further studies with mutants established the involvement of negatively charged glutamate and aspartate residues at the level of the cytoplasmic $K_{ir}2.1$ pore domain.[31,32,46] In the automated patch-clamp configuration, the time course for inhibition observed for such weak amine test articles applied externally results therefore from a combination of association kinetics at their internal sites of action and

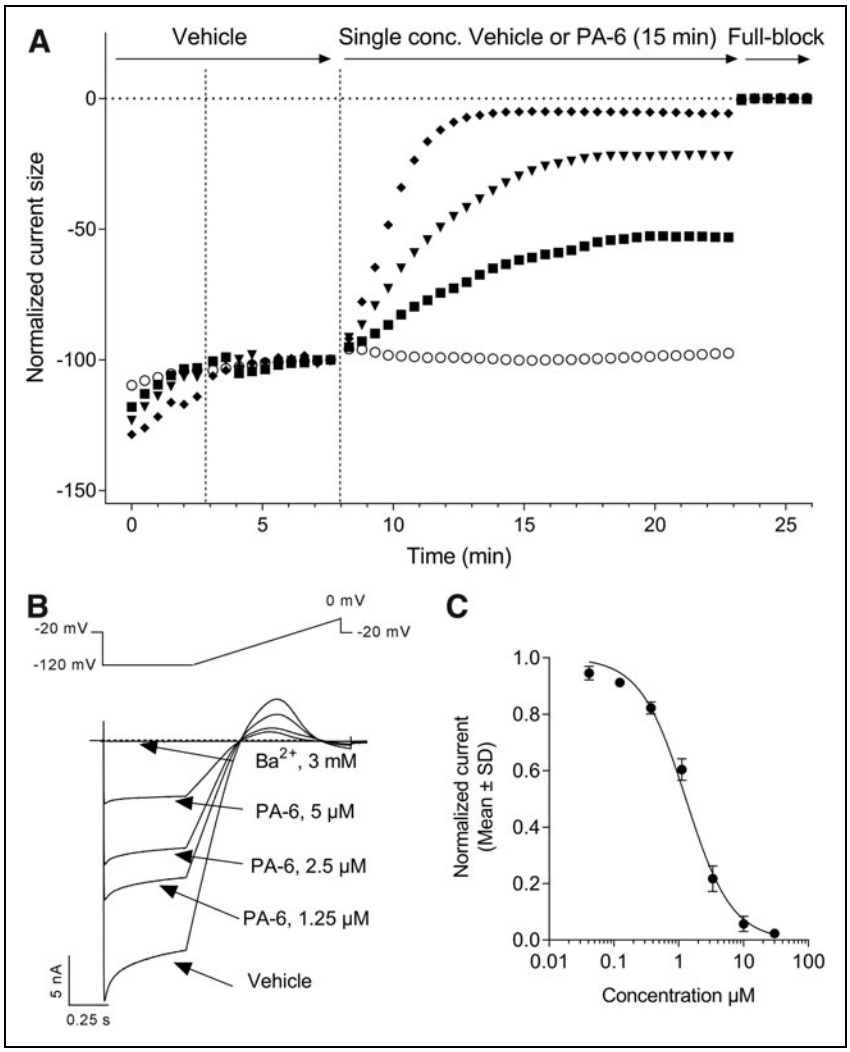

Fig. 6. Slow inhibition of $K_{ir}2.1$-mediated I_{K1} currents by the pentamidine derivative PA-6. **(A)** Four representative plots of steady-state current amplitude normalized with respect to baseline from multi-hole QPlates recordings are displayed. Induced CHO cells were first exposed to vehicle alone for the time period shown before the *vertical dashed line*. Then, in control experiments (*open circles*), the cells were exposed to vehicle alone, while in drug treatment recordings, the cells were exposed to vehicle containing 1.25 μM (*closed squares*), 5 μM (*closed triangles*), or 10 μM (*closed diamonds*) PA-6 (twofold dilution series). The inhibitory activity was allowed to develop over 15 min. The average two measurements at the end of the last vehicle period and the average five measurements at the end of a drug treatment period served for current amplitude normalization. A final episode in each experiment consisted in the application of a saturating concentration of Ba^{2+} as full block. **(B)** Representative multi-hole current traces in response to the voltage protocol shown above the traces. **(C)** Concentration–response curve for PA-6 inhibition using a threefold dilution series: IC_{50} was estimated from at least $N = 3$ wells per concentration applied individually. See *Table 1* for estimated value and 95% confidence interval.

membrane permeation of their uncharged molar fraction at neutral pH. Entry by organic cation transporters has been shown for pentamidine,[47] but it remains to be established whether such carriers are significantly expressed in CHO cells. We therefore adopted a noncumulative cell treatment protocol for the evaluation of PA-6, ML133, and chloroquine inhibitory potency. Cells were exposed to single concentrations of each compound in individual wells recorded in parallel. *Figure 6A* illustrates the time course of the effects of PA-6 when applied at concentrations ranging from 1.25 to 10 μM. Extension of the exposure duration to 15 min proved sufficient to reach stable inhibition for PA-6, ML133, and chloroquine. In contrast to Ba^{2+}, the inhibitory action of PA-6 on the $K_{ir}2.1$ current traces indicated no time dependency during the hyperpolarizing pulse, displaying identical inhibition on its instantaneous and steady-state components (*Fig. 6B*). The inhibitory potency of PA-6 calculated on the average current amplitudes collected over the five last voltage steps to −120 mV under drug exposure was $IC_{50} = 1.3$ μM (95% CI: 1.2–1.4 μM, $N = 3$–5, *Fig. 6B*) along with a Hill slope value near unity ($n_H = 1.2$, 95% CI: 1.2–1.4, *Table 1*). When tested with the same prolonged 15-min exposure protocol, ML133 and chloroquine yielded micromolar potencies (*Table 1*). Hill coefficients were close to 1, except for ML133, suggesting a cooperative mechanism of action for this compound independent of its slow kinetics of action as proposed by others.[31] These inhibitory activities are consistent with published data obtained using traditional manual patch-clamp. Thus, whole-cell $K_{ir}2.1$ currents elicited at −110 mV in *KCNJ2*-tranfected HEK cells were inhibited by 68% in the presence of 3 μM external PA-6,[48] whereas ML133 showed an IC_{50} value of 1.8 μM at −100 mV.[31] Similarly, in feline ventricular myocytes, 3 μM chloroquine decreased I_{K1} currents at −100 mV by 67%.[49]

Only a few small-molecule $K_{ir}2.1$ inhibitors have their molecular mechanism of action deciphered, and this was not an objective of this study. We rather extended our efforts to assess structurally diverse $K_{ir}2.1$-preferring or

Table 1. Potencies of $K_{ir}2.1$ Inhibitors

Test article	IC_{50} (95% CI) (μM)	Hill slope n_H (95% CI)
PA-6	1.3 (1.2–1.4)	1.2 (1.1–1.4)
ML133	1.2 (1.1–1.3)	2.6 (2.2–3.1)
Chloroquine	1.9 (1.8–2.1)	0.80 (0.76–0.83)
Chloroethylclonidine	46 (42–50)	0.81 (0.75–0.87)
Chlorpromazine	3.8 (3.4–4.2)	1.7 (1.4–2.1)
SKF-96365	4.7 (4.1–5.4)	1.3 (1.1–1.5)
Terikalant	8.4 (7.4–9.4)	0.98 (0.88–1.1)

CI, confidence interval; IC_{50}, half-maximal inhibitory concentrations.

multichannel inhibitors to generate a high-quality patch-clamp data set for further pharmacological assay or protocol comparisons. Chloroethylclonidine,[50] chlorpromazine,[51] SKF-96365,[52] and the class III antiarrhythmic agent terikalant[53] are known to affect $K_{ir}2.1$-mediated I_{K1} currents in recombinant or native cell systems at micromolar concentrations. We first screened them with the cumulative concentration application mode and observed slow inhibition kinetics for all of them, suggesting common actions at the cytoplasmic side of the $K_{ir}2.1$ channels. We therefore used the single-concentration noncumulative parallel application mode also for these four compounds; results of these quantitative evaluations are reported in *Table 1*. Only chloroethylclonidine appeared to reach fast-enough steady-state inhibition fitting a cumulative mode evaluation, which doubled its apparent potency with an IC_{50} value of 25 μM (95% CI: 23–28 μM, $N=3$) compared to the noncumulative application mode (data not shown).

Together with I_{Kr} and I_{Ks} currents flowing through the voltage-gated $K_v11.1$ and $K_v7.1$ channels, respectively, I_{K1} currents contribute to the "repolarization reserve" of the cardiac AP,[2,54] suggesting $K_{ir}2.1$ as a possible off-target for drug-induced cardiac side effects. Several screening assays for K_{ir} channels have previously been reported based on other readouts and formats. For example, a ratiometric fluorescence resonance energy transfer assay using cells in which K_{ir}-mediated potential changes are triggered by elevation of external $[K^+]_{out}$ could be miniaturized to a 1,536-well format.[55] However, although well suited for high-capacity screening, assays based on fluorescence readouts tend to generate significant numbers of false positives. Another screening format utilized yeast strains rendered unable to grow in low $[K^+]_{out}$ media by genetic cancellation of their endogenous K^+ transporters. Rescue of this phenotype by expression of mammalian $K_{ir}2.1$ and subsequent optical monitoring of yeast growth inhibition allowed the identification of a novel, although weak, catechol inhibitor.[56] However, expression of mammalian proteins in prokaryotic hosts could lead to folding alterations or yeast-specific glycosylations, which may potentially alter the channel pharmacology. Unfortunately, assays based on cardiomyocytes induced from human pluripotent stem cell cannot be used for the detection of $K_{ir}2.1$ inhibitors since they express insufficient amounts of I_{K1} to prevent them from spontaneously depolarizing and automatically beating.[57] Thus, the assay we describe in this study provides a useful tool for cardiovascular safety screening. Furthermore, it provides a platform for the discovery of novel $K_{ir}2.1$ channel ligands as drug candidates.

CONCLUSION

We have validated an automated patch-clamp assay for $K_{ir}2.1$ channels that reproduces cardinal features known for native I_{K1} currents and that generates concentration–response data for inhibitor tool compounds that agree with manual electrophysiology data. This assay is ready for cardiosafety screening of somewhat larger compound sets advancing toward preclinical development.

ACKNOWLEDGMENTS

We are grateful to Luc Bertin and Quentin Janet for the synthesis of PA-6, and to Drs. David Rampe and Rasmus Jacobsen for critical reading of the article before submission.

DISCLOSURE STATEMENT

The authors are current or former employees of Sanofi and declare no conflict of interests.

REFERENCES

1. Rampe D, Brown AM: A history of the role of the hERG channel in cardiac risk assessment. *J Pharmacol Toxicol Methods* 2013;68:13–22.
2. Roden DM: Predicting drug-induced QT prolongation and torsades de pointes. *J Physiol* 2016;594:2459–2468.
3. Food, Drug Administration HHS: International conference on HARMONISATION; guidance on E14 clinical evaluation of QT/QTc interval prolongation and proarrhythmic potential for non-antiarrhythmic drugs; availability. Notice. *Fed Regist* 2005;70:61134–61135.
4. Food, Drug Administration HHS: International conference on harmonisation; guidance on S7B nonclinical evaluation of the potential for delayed ventricular repolarization (QT interval prolongation) by human pharmaceuticals; availability. Notice. *Fed Regist* 2005;70:61133–61134.
5. Lu HR, Marien R, Saels A, De Clerck F: Species plays an important role in drug-induced prolongation of action potential duration and early afterdepolarizations in isolated Purkinje fibers. *J Cardiovasc Electrophysiol* 2001;12:93–102.
6. Redfern WS, Carlsson L, Davis AS, *et al.*: Relationships between preclinical cardiac electrophysiology, clinical QT interval prolongation and torsade de

pointes for a broad range of drugs: evidence for a provisional safety margin in drug development. *Cardiovasc Res* 2003;58:32–45.
7. Hammond TG, Carlsson L, Davis AS, *et al.*: Methods of collecting and evaluating non-clinical cardiac electrophysiology data in the pharmaceutical industry: results of an international survey. *Cardiovasc Res* 2001;49:741–750.
8. Lu HR, Vlaminckx E, Hermans AN, *et al.*: Predicting drug-induced changes in QT interval and arrhythmias: QT-shortening drugs point to gaps in the ICHS7B Guidelines. *Br J Pharmacol* 2008;154:1427–1438.
9. Gintant G: An evaluation of hERG current assay performance: translating preclinical safety studies to clinical QT prolongation. *Pharmacol Ther* 2011;129:109–119.
10. Kramer J, Obejero-Paz CA, Myatt G, *et al.*: MICE models: superior to the HERG model in predicting torsade de pointes. *Sci Rep* 2013;3:2100.
11. Fermini B, Hancox JC, Abi-Gerges N, *et al.*: A new perspective in the field of cardiac safety testing through the comprehensive in vitro proarrhythmia assay paradigm. *J Biomol Screen* 2016;21:1–11.
12. Gintant G, Sager PT, Stockbridge N: Evolution of strategies to improve preclinical cardiac safety testing. *Nat Rev Drug Discov* 2016;15:457–471.
13. Sager PT, Gintant G, Turner JR, Pettit S, Stockbridge N: Rechanneling the cardiac proarrhythmia safety paradigm: a meeting report from the Cardiac Safety Research Consortium. *Am Heart J* 2014;167:292–300.
14. Huang H, Pugsley MK, Fermini B, *et al.*: Cardiac voltage-gated ion channels in safety pharmacology: review of the landscape leading to the CiPA initiative. *J Pharmacol Toxicol Methods* 2017;87:11–23.
15. Millard D, Dang Q, Shi H, *et al.*: Cross-Site reliability of human induced pluripotent stem-cell derived cardiomyocyte based safety assays using microelectrode arrays: results from a blinded CiPA pilot study. *Toxicol Sci* 2018;164:550–562.
16. Lopatin AN, Makhina EN, Nichols CG: Potassium channel block by cytoplasmic polyamines as the mechanism of intrinsic rectification. *Nature* 1994;372:366–369.
17. Matsuda H, Saigusa A, Irisawa H: Ohmic conductance through the inwardly rectifying K channel and blocking by internal Mg2+. *Nature* 1987;325:156–159.
18. Stanfield PR, Nakajima S, Nakajima Y: Constitutively active and G-protein coupled inward rectifier K+ channels: Kir2.0 and Kir3.0. *Rev Physiol Biochem Pharmacol* 2002;145:47–179.
19. Hibino H, Inanobe A, Furutani K, Murakami S, Findlay I, Kurachi Y: Inwardly rectifying potassium channels: their structure, function, and physiological roles. *Physiol Rev* 2010;90:291–366.
20. de Boer TP, Houtman MJ, Compier M, van der Heyden MA: The mammalian K(IR)2.x inward rectifier ion channel family: expression pattern and pathophysiology. *Acta Physiol (Oxf)* 2010;199:243–256.
21. Hille B: *Ionic Channels of Excitable Membranes*. Sinauer Associates, Sunderland, MA, 1992.
22. Swale DR, Kharade SV, Denton JS: Cardiac and renal inward rectifier potassium channel pharmacology: emerging tools for integrative physiology and therapeutics. *Curr Opin Pharmacol* 2014;15:7–15.
23. Schram G, Pourrier M, Wang Z, White M, Nattel S: Barium block of Kir2 and human cardiac inward rectifier currents: evidence for subunit-heteromeric contribution to native currents. *Cardiovasc Res* 2003;59:328–338.
24. Nakamura TY, Artman M, Rudy B, Coetzee WA: Inhibition of rat ventricular IK1 with antisense oligonucleotides targeted to Kir2.1 mRNA. *Am J Physiol* 1998;274:H892–H900.
25. Zaritsky JJ, Redell JB, Tempel BL, Schwarz TL: The consequences of disrupting cardiac inwardly rectifying K(+) current (I(K1)) as revealed by the targeted deletion of the murine Kir2.1 and Kir2.2 genes. *J Physiol* 2001;533:697–710.
26. Miake J, Marban E, Nuss HB: Functional role of inward rectifier current in heart probed by Kir2.1 overexpression and dominant-negative suppression. *J Clin Invest* 2003;111:1529–1536.
27. Priori SG, Pandit SV, Rivolta I, *et al.*: A novel form of short QT syndrome (SQT3) is caused by a mutation in the *KCNJ2* gene. *Circ Res* 2005;96:800–807.
28. Tristani-Firouzi M, Jensen JL, Donaldson MR, *et al.*: Functional and clinical characterization of *KCNJ2* mutations associated with LQT7 (Andersen syndrome). *J Clin Invest* 2002;110:381–388.
29. Authier S, Pugsley MK, Koerner JE, *et al.*: Proarrhythmia liability assessment and the comprehensive in vitro proarrhythmia assay (CiPA): an industry survey on current practice. *J Pharmacol Toxicol Methods* 2017;86:34–43.
30. Korsgaard MP, Strobaek D, Christophersen P: Automated planar electrode electrophysiology in drug discovery: examples of the use of QPatch in basic characterization and high content screening on Na(v), K(Ca)2.3, and K(v)11.1 channels. *Comb Chem High Throughput Screen* 2009;12:51–63.
31. Wang HR, Wu M, Yu H, *et al.*: Selective inhibition of the K(ir)2 family of inward rectifier potassium channels by a small molecule probe: the discovery, SAR, and pharmacological characterization of ML133. *ACS Chem Biol* 2011;6:845–856.
32. Takanari H, Nalos L, Stary-Weinzinger A, *et al.*: Efficient and specific cardiac IK(1) inhibition by a new pentamidine analogue. *Cardiovasc Res* 2013;99:203–214.
33. Bakunova SM, Bakunov SA, Patrick DA, *et al.*: Structure-activity study of pentamidine analogues as antiprotozoal agents. *J Med Chem* 2009;52:2016–2035.
34. Houtmann S, Schombert B, Sanson C, Partiseti M, Bohme GA: Automated patch-clamp methods for the hERG cardiac potassium channel. *Methods Mol Biol* 2017;1641:187–199.
35. Dhamoon AS, Jalife J: The inward rectifier current (IK1) controls cardiac excitability and is involved in arrhythmogenesis. *Heart Rhythm* 2005;2:316–324.
36. Lopatin AN, Nichols CG: [K+] dependence of open-channel conductance in cloned inward rectifier potassium channels (IRK1, Kir2.1). *Biophys J* 1996;71:682–694.
37. Lopatin AN, Nichols CG: Inward rectifiers in the heart: an update on I(K1). *J Mol Cell Cardiol* 2001;33:625–638.
38. Isenberg G: Cardiac Purkinje fibers: cesium as a tool to block inward rectifying potassium currents. *Pflugers Arch* 1976;365:99–106.
39. Hagiwara S, Miyazaki S, Rosenthal NP: Potassium current and the effect of cesium on this current during anomalous rectification of the egg cell membrane of a starfish. *J Gen Physiol* 1976;67:621–638.
40. Hagiwara S, Miyazaki S, Moody W, Patlak J: Blocking effects of barium and hydrogen ions on the potassium current during anomalous rectification in the starfish egg. *J Physiol* 1978;279:167–185.
41. Gay LA, Stanfield PR: Cs(+) causes a voltage-dependent block of inward K currents in resting skeletal muscle fibres. *Nature* 1977;267:169–170.
42. Kubo Y, Baldwin TJ, Jan YN, Jan LY: Primary structure and functional expression of a mouse inward rectifier potassium channel. *Nature* 1993;362:127–133.
43. Shen N, Zheng J, Liu H, *et al.*: Barium chloride impaired Kir2.1 inward rectification in its stably transfected HEK 293 cell lines. *Eur J Pharmacol* 2014;730:164–170.
44. Abrams CJ, Davies NW, Shelton PA, Stanfield PR: The role of a single aspartate residue in ionic selectivity and block of a murine inward rectifier K+ channel Kir2.1. *J Physiol* 1996;493 (Pt 3):643–649.
45. Doupnik CA: Venom-derived peptides inhibiting Kir channels: past, present, and future. *Neuropharmacology* 2017;127:161–172.
46. Rodriguez-Menchaca AA, Navarro-Polanco RA, Ferrer-Villada T, *et al.*: The molecular basis of chloroquine block of the inward rectifier Kir2.1 channel. *Proc Natl Acad Sci U S A* 2008;105:1364–1368.
47. Ming X, Ju W, Wu H, Tidwell RR, Hall JE, Thakker DR: Transport of dicationic drugs pentamidine and furamidine by human organic cation transporters. *Drug Metab Dispos* 2009;37:424–430.

48. Ji Y, Veldhuis MG, Zandvoort J, *et al.*: PA-6 inhibits inward rectifier currents carried by V93I and D172N gain-of-function KIR2.1 channels, but increases channel protein expression. *J Biomed Sci* 2017;24:44.
49. Sanchez-Chapula JA, Salinas-Stefanon E, Torres-Jacome J, Benavides-Haro DE, Navarro-Polanco RA: Blockade of currents by the antimalarial drug chloroquine in feline ventricular myocytes. *J Pharmacol Exp Ther* 2001;297: 437–445.
50. Barrett-Jolley R, Dart C, Standen NB: Direct block of native and cloned (Kir2.1) inward rectifier K+ channels by chloroethylclonidine. *Br J Pharmacol* 1999;128: 760–766.
51. Crumb WJ, Jr., Vicente J, Johannesen L, Strauss DG: An evaluation of 30 clinical drugs against the comprehensive in vitro proarrhythmia assay (CiPA) proposed ion channel panel. *J Pharmacol Toxicol Methods* 2016;81: 251–262.
52. Liu H, Yang L, Chen KH, *et al.*: SKF-96365 blocks human ether-a-go-go-related gene potassium channels stably expressed in HEK 293 cells. *Pharmacol Res* 2016;104:61–69.
53. Escande D, Mestre M, Cavero I, Brugada J, Kirchhof C: RP 58866 and its active enantiomer RP 62719 (terikalant): blockers of the inward rectifier K+ current acting as pure class III antiarrhythmic agents. *J Cardiovasc Pharmacol* 1992;20 Suppl 2:S106–S113.
54. Roden DM: Taking the "idio" out of "idiosyncratic": predicting torsades de pointes. *Pacing Clin Electrophysiol* 1998;21:1029–1034.
55. Solly K, Cassaday J, Felix JP, *et al.*: Miniaturization and HTS of a FRET-based membrane potential assay for K(ir) channel inhibitors. *Assay Drug Dev Technol* 2008;6:225–234.
56. Zaks-Makhina E, Kim Y, Aizenman E, Levitan ES: Novel neuroprotective K+ channel inhibitor identified by high-throughput screening in yeast. *Mol Pharmacol* 2004;65:214–219.
57. Goversen B, van der Heyden MAG, van Veen TAB, de Boer TP: The immature electrophysiological phenotype of iPSC-CMs still hampers *in vitro* drug screening: Special focus on IK1. *Pharmacol Ther* 2018;183:127–136.

Address correspondence to:
G. Andrees Bohme, PharmD, PhD
Integrated Drug Discovery
High-Content Biology
Sanofi Research and Development
CRVA
13 Quai Jules Guesde BP14
Vitry-sur-Seine 94400
France

E-mail: andrees.bohme@sanofi.com

Abbreviations Used

AP = action potential
APD = action potential duration
CHO = Chinese hamster ovary
CI = confidence interval
DMSO = dimethyl sulfoxide
E_K = potassium equilibrium potential
IC_{50} = half-maximal inhibitory concentrations
I_{K1} = native inwardly rectifying current
$K_{ir}2.x$ = inward rectifier channel subunits—subfamily 2
LQT-7 = long QT syndrome—subtype 7
MTP = microtiter plates
QT = time interval between Q-wave and T-wave on the electrocardiogram
SQT-3 = Short QT syndrome–subtype 3
TdP = torsades de pointes
TQT = thorough QT